

Alternative LISA-TAIJI networks

Gang Wang,^{1,*} Wei-Tou Ni,^{2,3,†} Wen-Biao Han,^{1,4,5,‡} and Peng Xu^{6,7,5,§}

¹*Shanghai Astronomical Observatory, Chinese Academy of Sciences, Shanghai 200030, China*

²*State Key Laboratory of Magnetic Resonance and Atomic and Molecular Physics,
Innovation Academy for Precision Measurement Science and Technology (APM),
Chinese Academy of Sciences, Wuhan 430071, China*

³*Department of Physics, National Tsing Hua University, Hsinchu, Taiwan, 30013, ROC*

⁴*School of Astronomy and Space Science, University of Chinese Academy of Sciences, Beijing 100049, China*

⁵*Hangzhou Institute for Advanced Study, University of Chinese Academy of Sciences, Hangzhou 310124, China*

⁶*Institute of Mechanics, Chinese Academy of Sciences, Beijing 100190, China*

⁷*Lanzhou Center for Theoretical Physics, Lanzhou University, Lanzhou 730000, China*

(Dated: January 28, 2022)

The space-borne gravitational wave (GW) detectors, LISA and TAIJI, are planned to be launched in the 2030s. The dual detectors with comparable sensitivities will form a network observing GW with significant advantages. In this work, we report the investigations on the three possible LISA-TAIJI networks for different location and orientation compositions of LISA orbit (60° inclination and trailing the Earth by 20°) and alternative TAIJI orbit configurations including TAIJIp (60° inclination and leading the Earth by 20°), TAIJic (60° inclination and co-located with LISA), TAIJIm (−60° inclination and leading the Earth by 20°). In the three LISA-TAIJI configurations, the LISA-TAIJIm network shows a best performance on the sky localization and polarization determination for the massive binary system due to their complementary antenna pattern, and LISA-TAIJic could achieve the best cross correlation and observe the stochastic GW background with an optimal sensitivity.

I. INTRODUCTION

The gravitational wave detection, GW150914, was observed by Advanced LIGO detectors at two sites Hanford, WA and Livingston, LA [1]. Two interferometers are designed to be (closely) co-aligned interferometric arms with a separation of 3000 km. The GW170814 and GW170817 were the first detections simultaneously observed by triple interferometers of Advanced LIGO and Advanced Virgo. As profits from the mis-aligned Virgo orientation with LIGO, the source directions were well localized and the GW polarizations could be tested [2–4]. The KAGRA detector is expected to join the ground-based interferometer network in near future [5, 6]. The detector network surrounding the Earth will improve the angular resolution of the sky localization and parameter determination on the GW sources [6, 7]. Although the current GW detections are all from the compact binary coalescences, Advanced LIGO and Advanced Virgo are actively searching for the stochastic GW background (SGWB) [8–13]. The detection of the stochastic relic GW will deeply impact our understanding on the early Universe. To distinguish cosmological imprint from the instrument noise and astrophysical foreground, joint observation from two or more independent detectors would be demanded.

The multiple interferometer cooperation is also

planned in the next-generation space missions for GW observation in the middle frequency band. The present activities of missions for the GW detection in the middle frequency could be found in [14]. Both the BBO and DECIGO missions proposed three constellations deploying on the Earth-like heliocentric orbit with 120° separations [15, 16]. The number of detectors will increase the signal-to-noise ratio (SNR) of the detection, and the large separations between the constellations will improve their angular resolution of the sky localization for the sources. The SGWB could also be expected to be observed by the joint observation from the co-located interferometers of the BBO or DECIGO [17, 18].

The space-borne missions targeting for the milli-Hz low frequency band GW observation including LISA [19], TAIJI [20], and TianQin [21] are scheduled to be launched around the 2030s. Each of the missions will include a triangle constellation formed by three spacecraft (S/C). The LISA and TAIJI missions are designed to be heliocentric orbit. By assuming the TAIJI is leading the Earth by 20° and LISA is trailing the Earth by 20°, Ruan *et al.* [22] and Wang *et al.* [23] investigated the sky localization improvement of the LISA-TAIJI network compared to the single LISA mission. Omiya and Seto [24], Seto [25], and Orlando *et al.* [26] evaluated network capacities for the SGWB observation. Wang *et al.* [27] and Wang *et al.* [28] estimated the impact of the joint LISA-TAIJI observation on cosmological parameter determination. Wang and Han [29] demonstrated the observation constraint on the GW polarization from the joint observation.

Considering the orbital configuration of the TAIJI mission is not fully determined, the merits of the alternative

* Gang Wang: gwang@shao.ac.cn, gwanggw@gmail.com

† Wei-Tou Ni: weitou@gmail.com

‡ Wen-Biao Han: wbian@shao.ac.cn

§ Peng Xu: xp@lzu.edu.cn

LISA-TAIJI network are worth evaluating. In this work, by using the numerical mission orbits, we investigate the performances of three possible LISA-TAIJI network configuration for different TAIJI orbital selections as shown in Fig. 1, a) TAIJIp which leading the Earth by $\sim 20^\circ$ and the formation of the constellation is 60° inclined as LISA, b) TAIJIm which also leading the Earth by $\sim 20^\circ$ and the plane of the S/C has a -60° inclination compared to the LISA, and c) TAIJIC which is co-located and co-aligned with LISA and trailing the Earth by 20° . The deployment and observation for the TAIJI mission from these three orbit choices are expected to be not too much different. However, the joint observation with LISA from alternative TAIJI mission orbit could yield different performance for the supermassive black hole (SMBH) binary observation, and SGWB. We evaluate their sky localization for the SMBH binary, observations for the alternative polarizations beyond general relativity, and the overlap reduction function for the stochastic GW observations. In the three pairs combination, the LISA-TAIJIm network demonstrates a best parameter determinations for the SMBH binary observations, and LISA-TAIJIC shows an optimal capacity for the SGWB detection.

This paper is organized as follows. In Sec. II, we introduce three LISA-TAIJI network configurations and their joint sensitivities. In Sec. III, we report and compare the results of parameter determinations on the SMBH binary from three LISA-TAIJI networks including the angular resolution and the polarization observation. In Sec. IV, we investigate the overlap reduction functions of the three networks for the stochastic background. We recapitulate our conclusions in Sec. V. (We set $G = c = 1$ in this work except otherwise stated.).

II. ALTERNATIVE LISA-TAIJI NETWORK

A. The LISA and TAIJI orbital configurations

The LISA mission is scheduled to be launched in the 2030s which includes three S/C forming a 2.5×10^6 km triangle trailing the Earth by 20° [19]. The constellation plane has a 60° inclination with respect to the ecliptic plane as shown in Fig. 1. The TAIJI mission is proposed as a LISA-like orbital configuration with a 3×10^6 km arm length [20]. An assumed orbit for the TAIJI is that the constellation is in front of the Earth by 20° and has the same 60° inclination as LISA as shown in the left plot of Fig. 1. This TAIJI orbital configuration is labeled as TAIJIp, and multiple studies have been performed on the merits of this LISA-TAIJIp network for

the GW observations [22–24, 26, 29, 30].

The TAIJI orbital configuration could also have other choices without (or significant) increasing the launch budget. The first alternative is that the constellation formation is tuned to be -60° inclination compared to the LISA's $+60^\circ$ and we label it as TAIJIm. Another case would be that TAIJI is co-located and co-aligned with LISA which is named as TAIJIC in this work. The two orbital configurations are shown in the right panel of Fig. 1. For the LISA-TAIJIC network, their orientations of S/C formation would be co-aligned. For the LISA-TAIJIp, the angle between the two formations is $\sim 34.5^\circ$ and their separation angle will be $\sim 40^\circ$ and distance $\sim 1 \times 10^8$ km. And the angle of the orientation between the LISA and TAIJIm is around 71° with their antenna patterns better complementary to each other be shown in Fig. 2.

In this work, by employing the numerical orbits, we investigate the performances of three pairs of LISA-TAIJI networks (LISA-TAIJI, LISA-TAIJIm, and LISA-TAIJIC) on the detectability for SMBH binaries and the SGWB. The numerical orbits for the TAIJIp and TAIJIC are from our results in [23, 31], and the orbit for TAIJIm is newly obtained from our optimization method in [31–36].

B. Response formulation of TDI channel

For the space-borne GW missions, time-delay interferometry (TDI) is essential to suppress the laser frequency noise and achieve targeting sensitivity. The sensitivities for the different TDI channels have been evaluated numerically in our recent works [37, 38]. With the implementation of the TDI, the GW response is combined from the response in each evolved single link. The response functions to the GW tensor polarizations from general relativity in Doppler measurement have been formulated in [39–42]. And the response functions for the polarizations beyond the general relativity have been developed in Tinto and da Silva Alves [43]. To keep the integrity of the work, we reiterate the formulas of the response of TDI to the six polarizations as utilized in [29].

The GW propagation vector from a source locating at ecliptic longitude λ and latitude θ (in the solar-system barycentric coordinates) will be

$$\hat{k} = -(\cos \lambda \cos \theta, \sin \lambda \cos \theta, \sin \theta). \quad (1)$$

The polarization tensors of the GW signal for the $+$, \times , scalar breathing (b), scalar longitudinal (L), vector x and y, combining with the factors of the source's inclination angle ι are

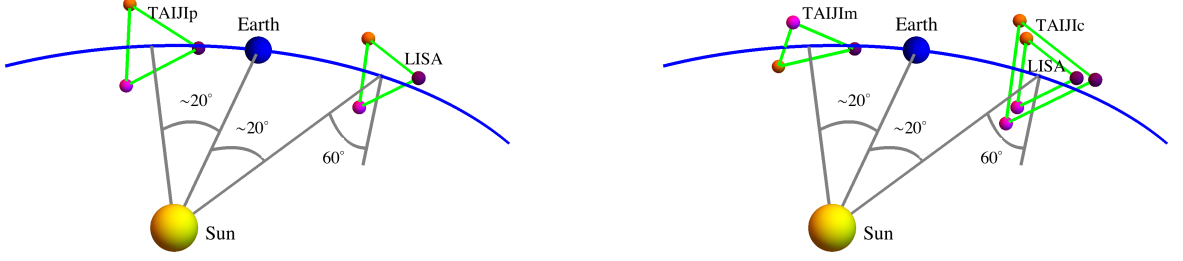


FIG. 1. The diagram of LISA and TAIJI mission orbital configurations. The left panel shows the fiducial LISA-TAIJIp network which the TAIJI has a $+60^\circ$ inclination with respect to the ecliptic plane. The right panel shows the LISA and two alternative TAIJI orbital choices which are the TAIJIm with the -60° inclination and TAIJlc formation plane co-located with the LISA. The angle between the LISA and TAIJIp formation planes is $\sim 34.5^\circ$, and the angle between the LISA and TAIJIm formation planes is $\sim 71^\circ$.

$$\begin{aligned}
 \mathbf{e}_+ &\equiv \mathcal{O}_1 \cdot \begin{pmatrix} 1 & 0 & 0 \\ 0 & -1 & 0 \\ 0 & 0 & 0 \end{pmatrix} \cdot \mathcal{O}_1^T \times \frac{1 + \cos^2 \iota}{2}, & \mathbf{e}_\times &\equiv \mathcal{O}_1 \cdot \begin{pmatrix} 0 & 1 & 0 \\ 1 & 0 & 0 \\ 0 & 0 & 0 \end{pmatrix} \cdot \mathcal{O}_1^T \times i(-\cos \iota), \\
 \mathbf{e}_b &\equiv \mathcal{O}_1 \cdot \begin{pmatrix} 1 & 0 & 0 \\ 0 & 1 & 0 \\ 0 & 0 & 0 \end{pmatrix} \cdot \mathcal{O}_1^T \times \sin^2 \iota, & \mathbf{e}_L &\equiv \mathcal{O}_1 \cdot \begin{pmatrix} 0 & 0 & 0 \\ 0 & 0 & 0 \\ 0 & 0 & 1 \end{pmatrix} \cdot \mathcal{O}_1^T \times \sin^2 \iota, \\
 \mathbf{e}_x &\equiv \mathcal{O}_1 \cdot \begin{pmatrix} 0 & 0 & 1 \\ 0 & 0 & 0 \\ 1 & 0 & 0 \end{pmatrix} \cdot \mathcal{O}_1^T \times \sin \iota \cos \iota, & \mathbf{e}_y &\equiv \mathcal{O}_1 \cdot \begin{pmatrix} 0 & 0 & 0 \\ 0 & 0 & 1 \\ 0 & 1 & 0 \end{pmatrix} \cdot \mathcal{O}_1^T \times i \sin \iota,
 \end{aligned} \tag{2}$$

with

$$\mathcal{O}_1 = \begin{pmatrix} \sin \lambda \cos \psi - \cos \lambda \sin \theta \sin \psi & -\sin \lambda \sin \psi - \cos \lambda \sin \theta \cos \psi & -\cos \lambda \cos \theta \\ -\cos \lambda \cos \psi - \sin \lambda \sin \theta \sin \psi & \cos \lambda \sin \psi - \sin \lambda \sin \theta \cos \psi & -\sin \lambda \cos \theta \\ \cos \theta \sin \psi & \cos \theta \cos \psi & -\sin \theta \end{pmatrix}, \tag{3}$$

where ψ is the polarization angle. The response to the GW polarization \mathbf{p} in the link from S/C*i* to *j* will be

$$y_{\mathbf{p},ij}^h(f) = \frac{\hat{\mathbf{n}}_{ij} \cdot \mathbf{e}_{\mathbf{p}} \cdot \hat{\mathbf{n}}_{ij}}{2(1 - \hat{\mathbf{n}}_{ij} \cdot \hat{\mathbf{k}})} \times \left[\exp(2\pi i f (L_{ij} + \hat{\mathbf{k}} \cdot \mathbf{p}_i)) - \exp(2\pi i f \hat{\mathbf{k}} \cdot \mathbf{p}_j) \right], \tag{4}$$

where $\hat{\mathbf{n}}_{ij}$ is the unit vector from S/C*i* to *j*, L_{ij} is the arm length from S/C*i* to *j*, \mathbf{p}_i is the position of the S/C*i* in the solar-system barycentric (SSB) ecliptic coordinates.

The first-generation Michelson TDI configuration and its corresponding optimal channels are employed to represent the performance of each mission. The response of the Michelson-X channel for a specific polarization \mathbf{p} in the frequency domain will be the sum of the responses in

the time shift single links,

$$\begin{aligned}
 F_{X,\mathbf{p}}(f) = & (-\Delta_{21} + \Delta_{21}\Delta_{13}\Delta_{31})y_{\mathbf{p},12}^h \\
 & + (-1 + \Delta_{13}\Delta_{31})y_{\mathbf{p},21}^h \\
 & + (\Delta_{31} - \Delta_{31}\Delta_{12}\Delta_{21})y_{\mathbf{p},13}^h \\
 & + (1 - \Delta_{12}\Delta_{21})y_{\mathbf{p},31}^h,
 \end{aligned} \tag{5}$$

where $\Delta_{ij} = \exp(2\pi i f L_{ij})$. The GW responses in the Michelson optimal A, E, and T channels are obtained by applying [41, 44]

$$\mathbf{A} = \frac{\mathbf{Z} - \mathbf{X}}{\sqrt{2}}, \quad \mathbf{E} = \frac{\mathbf{X} - 2\mathbf{Y} + \mathbf{Z}}{\sqrt{6}}, \quad \mathbf{T} = \frac{\mathbf{X} + \mathbf{Y} + \mathbf{Z}}{\sqrt{3}}, \tag{6}$$

where Y and Z channels are obtained from cyclical permutation of the S/C indexes in the X channel.

C. The sensitivity of the networks

1. The noises in TDI

Multiple sources of noise will be involved in the process of TDI combinations. For the Michelson-X channels, the expression of measurements could be described as [42],

$$X = [\mathcal{D}_{31}\mathcal{D}_{13}\mathcal{D}_{21}\eta_{12} + \mathcal{D}_{31}\mathcal{D}_{13}\eta_{21} + \mathcal{D}_{31}\eta_{13} + \eta_{31}] - [\eta_{21} + \mathcal{D}_{21}\eta_{12} + \mathcal{D}_{21}\mathcal{D}_{12}\eta_{31} + \mathcal{D}_{21}\mathcal{D}_{12}\mathcal{D}_{31}\eta_{13}] \quad (7)$$

where \mathcal{D}_{ij} is a time-delay operator, $\mathcal{D}_{ij}\eta(t) = \eta(t - L_{ij})$, η_{ji} are the combined observables from S/Cj to S/Ci [45–47], and the specific expressions for this work are defined in [38]. By assuming the dominant laser frequency noises are sufficiently suppressed, the acceleration noise and optical path noise in η_{ij} are incorporated in the noise estimation.

The noise budgets for the acceleration noise S_{acc} are assumed to be the same for the LISA and TAIJI as specified in [19, 48],

$$S_{\text{acc}}^{1/2} = 3 \times 10^{-15} \frac{\text{m/s}^2}{\sqrt{\text{Hz}}} \sqrt{1 + \left(\frac{0.4\text{mHz}}{f}\right)^2} \sqrt{1 + \left(\frac{f}{8\text{mHz}}\right)^4}. \quad (8)$$

And the optical path noises S_{op} requirement for two missions are treated slightly different as

$$S_{\text{op,LISA}}^{1/2} = 10 \times 10^{-12} \frac{\text{m}}{\sqrt{\text{Hz}}} \sqrt{1 + \left(\frac{2\text{mHz}}{f}\right)^4}, \quad (9)$$

$$S_{\text{op,TAIJI}}^{1/2} = 8 \times 10^{-12} \frac{\text{m}}{\sqrt{\text{Hz}}} \sqrt{1 + \left(\frac{2\text{mHz}}{f}\right)^4}.$$

And the power spectrum density (PSD) of a TDI channel $S_{\text{n,TDI}}$ is obtained by implementing the algorithm in [37, 38].

2. The joint sensitivities

The antenna pattern of one interferometer will change with the four geometric angles $\Omega(\lambda, \theta, \psi, \iota)$ and the frequency. For a given Ω and frequency, the sensitivities of the LISA's A+E+T channel and joint LISA-TAIJI network at a given mission time could be evaluated respectively by,

$$S_{\text{LISA}}^{1/2}(f, \Omega) = \left(\sum_{\text{A,E,T}} \frac{|F_{\text{TDI}}(f, \Omega)|^2}{S_{\text{n,TDI}}(f)} \right)^{-1/2}, \quad (10)$$

$$S_{\text{joint}}^{1/2}(f, \Omega) = \left(\sum_{\text{LISA}} \sum_{\text{A,E,T}} \frac{|F_{\text{TDI}}(f, \Omega)|^2}{S_{\text{n,TDI}}(f)} \right)^{-1/2}. \quad (11)$$

The sensitivities to the tensor polarizations from the LISA and joint LISA-TAIJI networks for $\psi = 0, \iota = 0$, and $f = 10$ mHz are shown in Fig. 2. As we can see in the upper left plot, the LISA has the optimum sensitivity around the normal directions of the triangular formation plane considering its 60° inclination. As expected from Fig. 1, the antenna pattern of the TAIJIp is shifted by $\sim 40^\circ$ along the ecliptic latitude with respect to the LISA's. And their joint sensitivity is shown by the upper right panel in Fig. 2. For the TAIJI_m, due to its 40° separation and -60° inclination with respect to the LISA, its antenna pattern is not only shifted by 40° along the latitude, also inversed with respect to the ecliptic plane. And their joint sensitivity of the LISA-TAIJI_m is shown in the lower left panel. As for the TAIJI_c case, since the TAIJI_c is co-located with LISA, the joint LISA-TAIJI_c enhanced the LISA's sensitivity as shown in the lower right plot.

III. PARAMETER DETERMINATIONS FOR SMBH BINARY COALESCENCE

As the most promising GW source for the LISA and TAIJI missions, the SMBH binary is selected to demonstrate the performances of parameter determination from the three LISA-TAIJI networks.

A. Fisher information method

The Fisher information matrix (FIM) is employed in this investigation to determine the uncertainty of parameters from GW observation [49–52, and references therein]. For a single mission with full six links, the FIM is combined from the three optimal channels (A, E, and T). The FIM of the joint LISA-TAIJI network is obtained by summing up the FIM from two missions,

$$\Gamma_{ij} = \sum_{\text{LISA}}^{\text{TAIJI}} \sum_{\text{A,E,T}} \left(\frac{\partial \tilde{h}_{\text{TDI}}}{\partial \xi_i} \middle| \frac{\partial \tilde{h}_{\text{TDI}}}{\partial \xi_j} \right), \quad (12)$$

with

$$(g|h)_{\text{TDI}} = 4\text{Re} \int_0^\infty \frac{g^*(f)h(f)}{S_{\text{TDI}}(f)} df, \quad (13)$$

where \tilde{h}_{TDI} is the frequency domain GW waveform responded in a TDI channel, ξ_i is the i -th parameter to be determined, and $S_{\text{TDI}}(f)$ is the noise PSD of the corresponding TDI channel.

Considering the sky location estimation will be significantly affected by the polarization content of the source [2–4], only tensor polarizations from GR are included for the FIM implementation to investigate the angular resolution of the sky localization. There are 9 parameters included describing the GW signal and TDI responses from LISA or LISA-TAIJI network, which are ecliptic

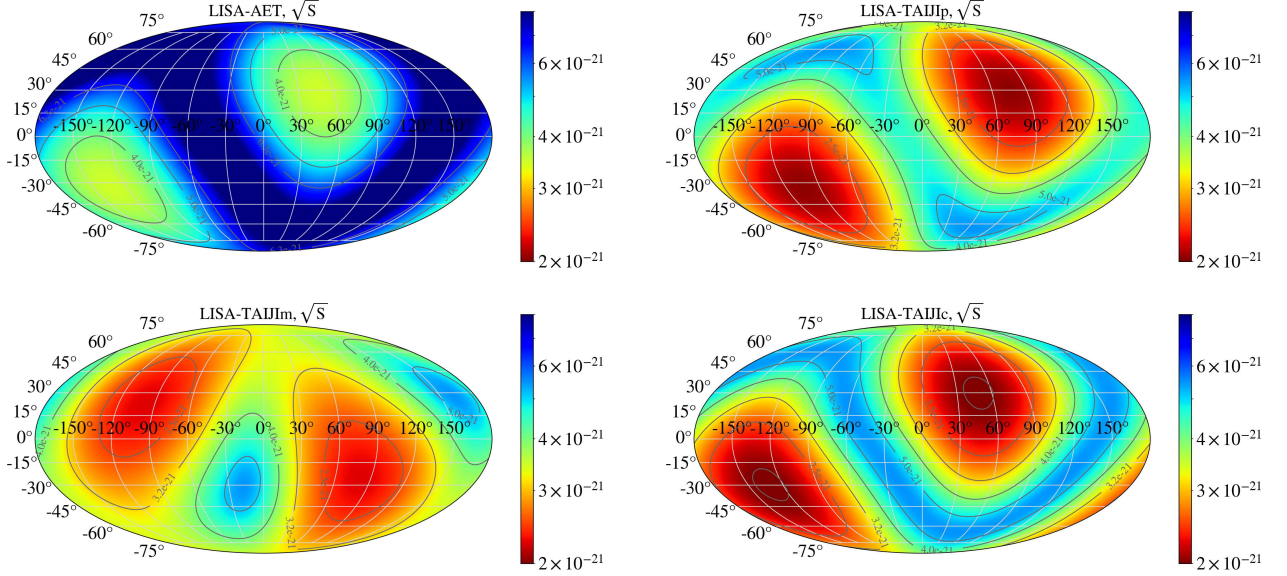


FIG. 2. The instantaneous sensitivities on the sky map for the LISA mission and LISA-TAIJI networks at $\psi = 0, \iota = 0$, and $f = 10\text{mHz}$. The single LISA sensitivity is shown by the upper left panel using Eq. (10). The joint LISA-TAIJI network sensitivities are obtained by using Eq. (11). The sensitivity of the LISA-TAIJIp is shown in the upper right panel, the sensitivity of LISA-TAIJIm is shown in the lower left panel, and the sensitivity of the LISA-TAIJlc is shown by the lower right panel. The plots reflect the antenna pattern of the detectors considering the orientation of the S/C formations. The LISA-TAIJIm network achieves a better averaged sensitivity to the different sky directions than the other two networks.

longitude and latitude (λ, θ) , polarization angle ψ , source inclination ι , luminosity distance D , the coalescence time and phase (t_c, ϕ_c) , the total mass of binary M and mass ratio q . The TDI responded GW signal incorporating two polarizations (+ and \times) could be described as

$$\tilde{h}_{\text{GR,TDI}}(f) = (F_+ + F_\times) \tilde{h}_{\text{GR}}, \quad (14)$$

where $h_{\text{GR,TDI}}$ is the frequency domain waveform represented by IMRPhenomPv2 [53]. When the investigations on the constraint on the GW alternative polarizations are performed, additional 6 ppE (parametrized post-Einsteinian) parameters, $(\beta, b, \alpha_b, \alpha_L, \alpha_\times, \alpha_\times)$, are considered to qualify the deviations from the general relativity as developed in [54], and the waveform will be explained in Eq. (18).

The variance-covariance matrix of the parameters is calculated by

$$\langle \Delta \xi_i \Delta \xi_j \rangle = (\Gamma^{-1})_{ij} + \mathcal{O}(\rho^{-1}) \stackrel{\rho \gg 1}{\simeq} (\Gamma^{-1})_{ij}. \quad (15)$$

The standard deviations σ_i and correlation σ_{ij} of the parameters for the high SNR $\rho \gg 1$ will be

$$\begin{aligned} \sigma_i &\simeq \sqrt{(\Gamma^{-1})_{ii}}, \\ \sigma_{ij} &= \text{cov}(\xi_i, \xi_j) \simeq (\Gamma^{-1})_{ij}. \end{aligned} \quad (16)$$

The uncertainties of the sky localization is evaluated by

$$\Delta \Omega \simeq 2\pi |\cos \theta| \sqrt{\sigma_\lambda \sigma_\theta - \sigma_{\lambda\theta}^2}. \quad (17)$$

The Monte Carlo simulation is performed for parameter determination by 1000 sources. The (λ, θ) are randomly sampled in the sky sphere, ψ is sampled in $[0, 2\pi]$ uniformly, $\cos \iota$ is sampled randomly in $[-1, 1]$, the merge time t_c is randomly in one year. The $m_1 = 10^5 M_\odot, q = 1/3$ at redshift $z = 2$ is employed as we used in [23, 29]. Considering that the SNR is mainly contributed from in the binary coalescing stage, the 30 days observation before the merge is simulated to perform the investigation.

B. Sky localization of the networks

The cumulative histograms of SNR from the LISA and LISA-TAIJI networks are shown in the left panel of Fig. 3. Compared to the single LISA mission, three LISA-TAIJI networks achieved more than $\sqrt{2}$ SNR as expected since the TAIJI is more sensitive to LISA in the selected GW frequency band. In the three networks, the LISA-TAIJlc has a larger range of the SNR distribution with a longer tail, because the co-aligned detectors are sensitive/insensitive to the same directions and leaving the common optimal/blind areas. The LISA-TAIJIm shows the most concentrated SNRs values compared to the two other networks since their joint antenna pattern is better complementary and has more averaged sensitivities to the sky areas as shown in Fig. 2.

The angular resolutions of the sky localization from the LISA and LISA-TAIJI networks are shown in the right panel of Fig. 3. For the LISA-TAIJlc network, the

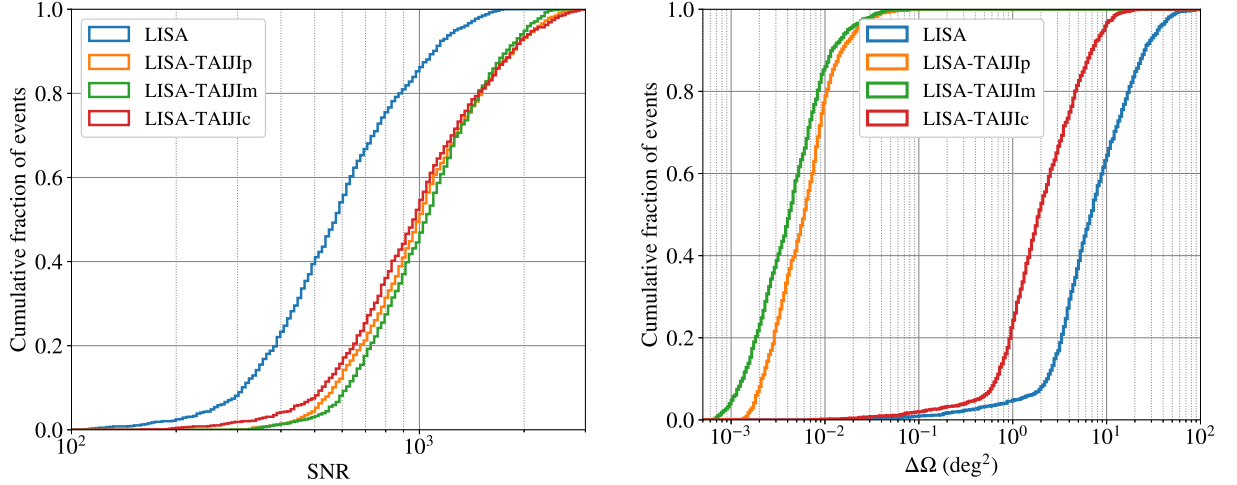


FIG. 3. The cumulative histograms of SNR (left panel) and angular resolutions of the sky localization (right panel) from the LISA and three LISA-TAIJI networks. Three LISA-TAIJI networks could achieve more than $\sqrt{2}$ SNR of LISA mission. In the three networks, the SNR from LISA-TAIJIm has the most concentrated distribution because of the most averaged antenna pattern as shown in Fig. 2. The distribution of SNR from LISA-TAIJlc has a long tail since the two missions have the same insensitive areas. On the right plot, the resolution of sky localization by LISA-TAIJlc is approximately twice better than the single LISA as the attribute to the SNR increase. The angular resolution of the LISA-TAIJIp is better than LISA-TAIJlc since the long baseline separation. The performance of LISA-TAIJIm is better than LISA-TAIJIp because the angle of the LISA and TAIJIm formation planes is 71° and their orientation could better compensate for each other's antenna pattern.

uncertainties of sky localization are improved by more than 2 times compared to the single LISA mission which should due to the more than $\sqrt{2}$ times SNR from the network to the LISA. Compared to the LISA-TAIJlc, the joint observation from LISA-TAIJIp demonstrate the more than 2 orders improvement on the localization resolution which should attribute to the long baseline separations between the LISA and TAIJIp. On the other side, the LISA-TAIJIm yield a better capability on locating the source than LISA-TAIJIp because the TAIJIm's formation plane is 71° with respect to LISA's and its antenna pattern could better compensate the LISA's insensitive directions.

C. Observation for GW polarizations

The detector responded GW signal is modified as follows to incorporate alternative polarization beyond general relativity [29, 54],

$$\begin{aligned} \tilde{h}_{\text{ppE,TDI}}(f) = & [(F_+ + F_\times)(1 + c\beta u_2^{b+5}) + \alpha_b F_b + \alpha_L F_L \\ & + \alpha_x F_x + \alpha_y F_y] \tilde{h}_{\text{GR}} e^{2i\beta u_2^b}, \end{aligned} \quad (18)$$

where c is the function of b is defined by Eq. (11) in the Erratum [55] of [54], \tilde{h}_{GR} is the GW waveform from GR in frequency domain, and $u_2 \equiv (\pi \mathcal{M} f)^{1/3}$. In this investigation, we choose $b = -3$ which correspond to the massive graviton theory [56–62], and set $\beta = 0.01$ which is from the rough boundary constrained in [63]. Although

this specific selection could not represent all other gravity theories, we have demonstrated that the measurement on the (b, β) values could also be similarly improved by the LISA-TAIJI network for other values [29]. The other four ppE parameters tuning the amplitudes of the alternative polarizations are set to be zeros, $(\alpha_b, \alpha_L, \alpha_x, \alpha_y) = (0, 0, 0, 0)$.

The constraints on the ppE parameters α for the scalar (upper panel) and vector (lower panel) polarizations are shown in Fig. 4. Similar to the results achieved for the sky localization, the constraint on α from the LISA-TAIJlc is more than $\sqrt{2}$ times better than single LISA which is an attribute from the increase of SNR. The LISA-TAIJIp, with large separation, could resolve other parameters of the sources and then help improve the constraint on the polarization significantly. And LISA-TAIJIm could achieve the best constraints on the polarizations in the three LISA-TAIJI configurations as the benefit of better antenna pattern cooperation.

IV. OVERLAP REDUCTION FUNCTION OF THE LISA-TAIJI NETWORK

The response of the detector network to the stochastic background GW signal will depend on the positions and orientations of the interferometers. Flanagan [64] evaluated the sensitivities of the ground-based GW interferometers to the stochastic background. An *overlap reduction function* is introduced to indicate the cross-correlation

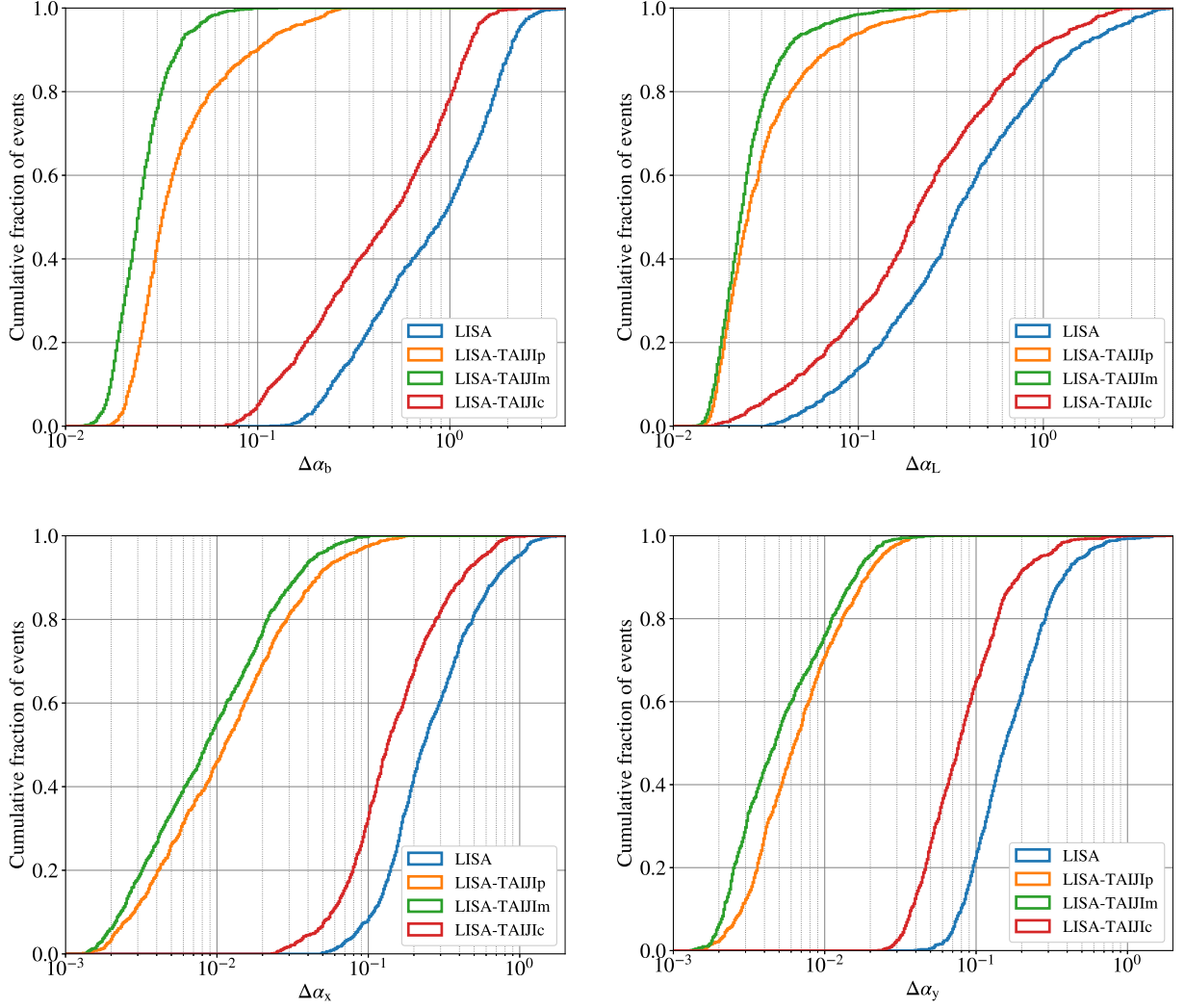


FIG. 4. The cumulative histograms of the constraints on the scalar and vector polarizations. The results from the LISA-TAIJIc is more than $\sqrt{2}$ times better than the single LISA which is an attribute from the increase of SNR. The LISA-TAIJIp could resolve other parameters of the sources and then help improve the constraint on polarizations significantly. And LISA-TAIJIm achieve the best constraints on the polarizations in the three LISA-TAIJI configurations as the benefit of the better antenna pattern cooperation.

between a pair of detectors [65]. Whelan *et al.* [66] calculated the overlap reduction functions for the two LIGO detectors and GEO. Omiya and Seto [24], Seto [25], and Orlando *et al.* [26] specify the overlap function of the LISA-TAIJIp network for optimal TDI channels and alternative GW polarizations. Schmitz [18] review the detectability of the ground- and space-based detectors for the stochastic GW background.

For a single LISA-like mission with full six measurement links, three equivalent interferometers from optimal TDI channels could be formed. The observation from these TDI channels could also be used to detect the stochastic GW background [67]. And the motion of the detectors may also help to resolve the background, especially for the anisotropic signal [17]. The LISA and

TAIJI could form an ideal network to separate the cosmological SGWB signal from other stochastic processes such as the instrument noise and astrophysical foreground.

To characterize the cross-correlation between LISA and different TAIJI orbital configurations, their overlap reduction functions are calculated for different polarizations,

$$\gamma_{ab,p}(f) = \frac{\kappa}{4\pi} \int d\mathbf{n} \left(\sum_{A,E,T} F_{\text{TDI},p}^a(f, \mathbf{n}) \right) \left(\sum_{A,E,T} F_{\text{TDI},p}^b(f, \mathbf{n}) \right) \quad (19)$$

where $F_{\text{TDI},p}^a$ is the response function to the polarization p (tensor, vector, scalar breathing mode, and scalar longitudinal mode) in the TDI channel from the mission a ,

and κ is the normalization factor to make $\gamma_{ab} = 1$ when the two detectors are co-aligned and co-localized. The polarization angle ψ is set to be zero, and inclination ι is set to be optimal for each polarization mode.

The overlap reduction functions for the different LISA-TAIJI networks for different polarizations are shown in Fig. 5. Since the orientations of the LISA and TAIJic are aligned and locations of them are at the same place, the overlap function of the LISA-TAIJic network is unity for the frequency lower than 10 mHz which indicates the strong correlation between the LISA and TAIJic detectors, and the network is optimal for the SGWB observation for all polarization modes. Considering the 1×10^8 km separation between LISA and TAIJIp/TAIJIm, the overlap reduction functions quickly are close to zero around a critical frequency $f_{\text{crit}} \simeq c/(2 \times 1 \times 10^8 \text{ km}) \simeq 1.5 \text{ mHz}$ [17], and oscillate and decay with the frequency increase. The γ_{ab} from the LISA-TAIJIp pair is higher than the value of the LISA-TAIJIm because the orientation of the LISA is more aligned with the TAIJIp (34.5°) than the TAIJIm (71°) to make TAIJIp has a stronger correlation with the LISA. Therefore, in the three LISA-TAIJI networks, the LISA-TAIJIm is the relatively worst configuration for the SGWB detections.

There is a trade-off for a LISA-like GW detector network to observe the compact binary system and SGWB. A long baseline for detectors deployment will promote the parameter resolutions. However, the frequency for the detectable SGWB band will be lowered,

$$f_{\text{crit}} = \frac{c}{2d} = \frac{c}{2 \times 2\text{AU} \sin \frac{\epsilon}{2}} \simeq \frac{0.5 \text{ mHz}}{\sin \frac{\epsilon}{2}} \quad (20)$$

where c is the speed of the light here, d is the distance between two detectors, ϵ is the separation angle formed by the two lines connecting the Sun and detector. On the other side, the angle between the constellation plane also changes with the separation angle as shown in Fig. 6. The orientation of the plane with an angle closing to 90° would be helpful to resolve the source parameters. The composition with an inversed inclination, a $+60^\circ$ together with a -60° inclination, could more cooperative than the two missions with a same inclination for a separation angle small than 90° . For the BBO or DECIGO mission, the constellations are planned to be separated by 120° , and there would be two options for their orientation deployment, 83° or 51° with respect to another formation plane as tagged in Fig. 6.

V. CONCLUSIONS

In this work, we investigate the performances of three possible LISA-TAIJI networks on the sky localizations and polarization observations from the supermassive black hole binary and capacity of the stochastic gravi-

tational wave background detections. For the observation of the binary system, compared to the single LISA mission, the co-located and co-aligned LISA-TAIJic network ordinarily increase the SNRs by a factor of $\sqrt{2}$. With a large separation, the joint observations from LISA and TAIJIp significantly improve parameter determinations of the sources than the LISA-TAIJic. The LISA-TAIJIm network demonstrates a better detectability to resolve the sky localization and polarizations than the LISA-TAIJIp network as a profit of more mis-aligned orientation and complementary antenna pattern. For the detectability for the stochastic gravitational wave background, the LISA-TAIJic would have optimal performance as the benefit of the aligned orientation and co-location, the TAIJIm present the worst correlation with the LISA due to the least aligned orientation with the LISA in the three TAIJI orbital configurations.

One lesson from this investigation for different LISA-TAIJI networks is that the parameter resolution of the compact binary coalescences will be impacted by the SNR, distance of detector separation, and the cooperative orientations of the detectors. The next generation space GW detectors, both DECIGO and BBO, proposed LISA-like heliocentric orbit with multiple constellations and is targeting to detect the relic GW left by the Big Bang, intermediate mass black holes, etc [15, 16]. The parameter resolution improvements have been performed for the compact binaries in [15] as the results of the multiple interferometers and long-baseline. The orientations of the constellations are also worth to be evaluated for the targeting sources.

Beyond the LISA-like orbital formation, various space missions are proposed to arrange S/C equally on a planet orbit in order to observe GW in the μHz GW band, for instance, ASTROD-GW [68], Folkner mission [69], μAres [70], etc. The ASTROD-GW is initially proposed to deploy 3 S/C around the Lagrange points L3, L4, and L5 of the Sun-Earth system, and an extended deployment could be 6 S/C to form two triangular interferometers to enhance the sensitivity to the SGWB [68]. The μAres will place the two orthogonal triangle interferometers with respect to the Mars (or Earth/Venus) orbit. The trade-off of detectability from various deployments could also be explored to balance the GW observations from the compact binary systems and resolve the stochastic background.

ACKNOWLEDGMENTS

This work was supported by NSFC Nos. 12003059 and 11773059, the Strategic Priority Research Program of the Chinese Academy of Sciences under Grants No. XDA15021102. This work made use of the High Performance Computing Resource in the Core Facility for Advanced Research Computing at Shanghai Astronomical Observatory.

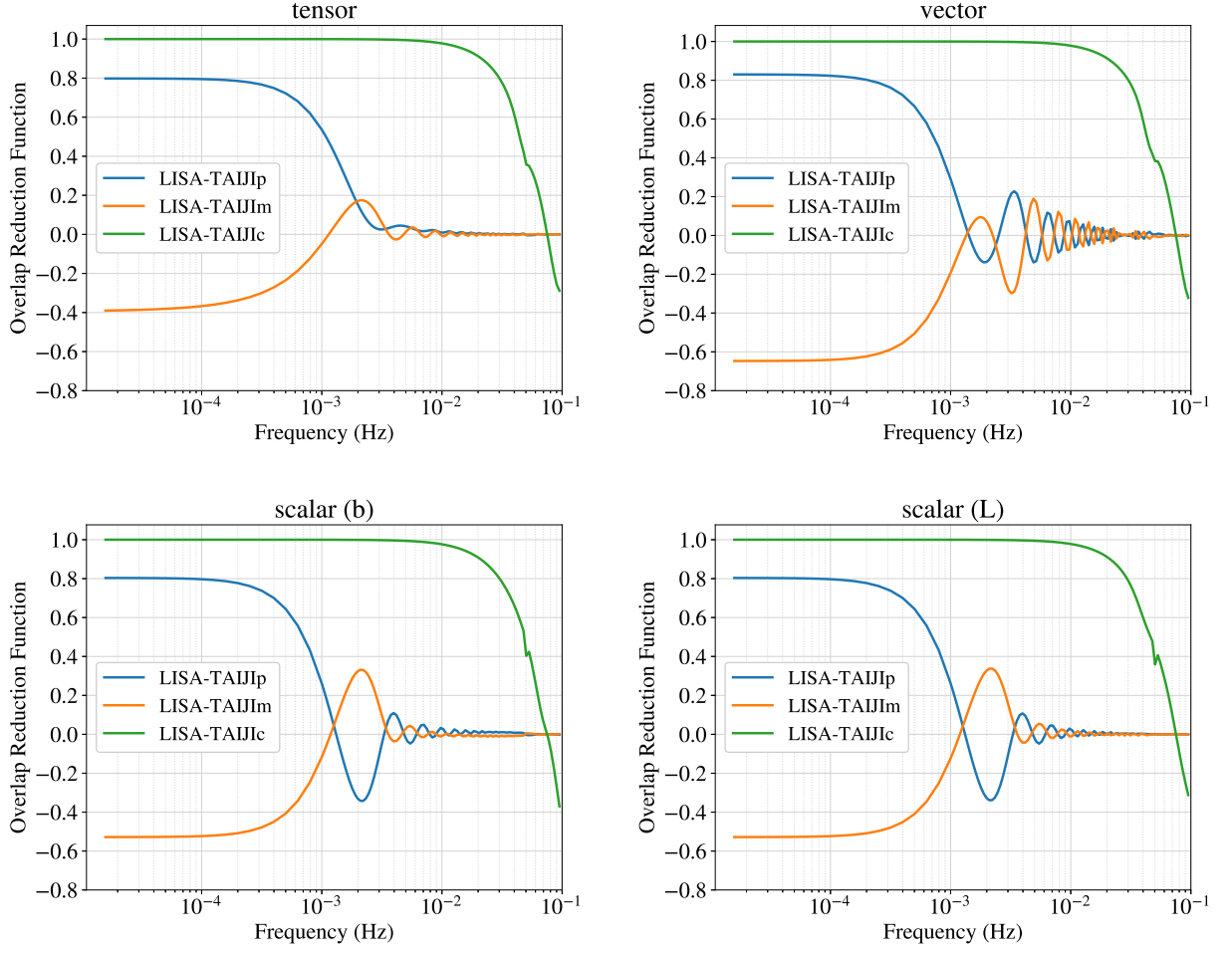


FIG. 5. The overlap reduction functions of three LISA-TAIJI networks for different polarization modes. The overlap function of the LISA-TAIJIc network is unity for the frequency lower than 10 mHz which is optimal for the SGWB observation. The overlap functions of the LISA-TAIJIp/TAIJIIm are close to zero around 1.5 mHz due to their $d = 1 \times 10^8$ km separations ($f_{\text{crit}} \simeq c/(2 \times 1 \times 10^8 \text{ km}) \simeq 1.5 \text{ mHz}$). The LISA-TAIJIIm pair has the worse cross-correlation than the LISA-TAIJIp because of the more mis-aligned orientation.

-
- [1] B. P. Abbott *et al.* (LIGO Scientific, Virgo), Observation of Gravitational Waves from a Binary Black Hole Merger, *Phys. Rev. Lett.* **116**, 061102 (2016), arXiv:1602.03837 [gr-qc].
 - [2] B. P. Abbott *et al.* (LIGO Scientific, Virgo), GW170814: A Three-Detector Observation of Gravitational Waves from a Binary Black Hole Coalescence, *Phys. Rev. Lett.* **119**, 141101 (2017), arXiv:1709.09660 [gr-qc].
 - [3] B. P. Abbott *et al.* (LIGO Scientific, Virgo), GW170817: Observation of Gravitational Waves from a Binary Neutron Star Inspiral, *Phys. Rev. Lett.* **119**, 161101 (2017), arXiv:1710.05832 [gr-qc].
 - [4] B. P. Abbott *et al.* (LIGO Scientific, Virgo), Tests of General Relativity with GW170817, *Phys. Rev. Lett.* **123**, 011102 (2019), arXiv:1811.00364 [gr-qc].
 - [5] T. Akutsu *et al.* (KAGRA), Overview of KAGRA : KAGRA science, (2020), arXiv:2008.02921 [gr-qc].
 - [6] B. P. Abbott *et al.* (KAGRA, LIGO Scientific, Virgo), Prospects for observing and localizing gravitational-wave transients with Advanced LIGO, Advanced Virgo and KAGRA, *Living Rev. Rel.* **23**, 3 (2020).
 - [7] B. F. Schutz, Networks of gravitational wave detectors and three figures of merit, *Class. Quant. Grav.* **28**, 125023 (2011), arXiv:1102.5421 [astro-ph.IM].
 - [8] B. P. Abbott *et al.* (LIGO Scientific, Virgo), Upper Limits on the Stochastic Gravitational-Wave Background from Advanced LIGO's First Observing Run, *Phys. Rev. Lett.* **118**, 121101 (2017), [Erratum: *Phys. Rev. Lett.* **119**, 029901 (2017)], arXiv:1612.02029 [gr-qc].
 - [9] B. P. Abbott *et al.* (LIGO Scientific, Virgo),

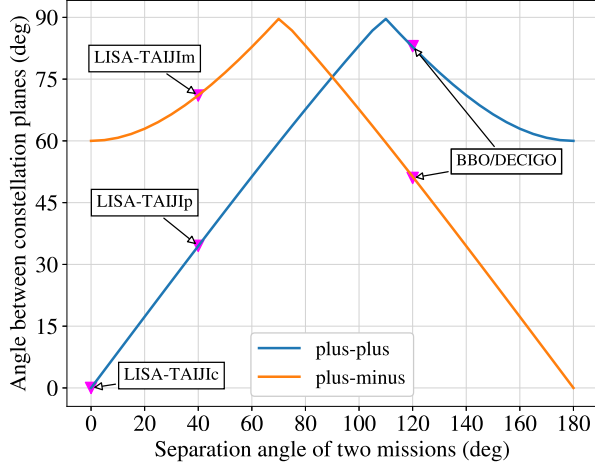


FIG. 6. The angle between the constellation planes varying with the separation angle of two missions. The curve of the plus-plus indicates the two missions having $+60^\circ$ inclination with respect to the ecliptic plane, and the curve of the plus-minus indicates that one mission having $+60^\circ$ inclination and another having a -60° inclination.

- Search for Tensor, Vector, and Scalar Polarizations in the Stochastic Gravitational-Wave Background, *Phys. Rev. Lett.* **120**, 201102 (2018), arXiv:1802.10194 [gr-qc].
- [10] B. P. Abbott *et al.* (LIGO Scientific, Virgo), Search for the isotropic stochastic background using data from Advanced LIGO's second observing run, *Phys. Rev. D* **100**, 061101 (2019), arXiv:1903.02886 [gr-qc].
- [11] R. Abbott *et al.* (LIGO Scientific, Virgo, KAGRA), Upper Limits on the Isotropic Gravitational-Wave Background from Advanced LIGO's and Advanced Virgo's Third Observing Run, (2021), arXiv:2101.12130 [gr-qc].
- [12] R. Abbott *et al.* (LIGO Scientific, Virgo, KAGRA), Constraints on cosmic strings using data from the third Advanced LIGO-Virgo observing run, (2021), arXiv:2101.12248 [gr-qc].
- [13] R. Abbott *et al.* (LIGO Scientific, Virgo, KAGRA), Search for anisotropic gravitational-wave backgrounds using data from Advanced LIGO's and Advanced Virgo's first three observing runs, (2021), arXiv:2103.08520 [gr-qc].
- [14] W.-T. Ni, Mid-frequency gravitational wave detection and sources, *Int. J. Mod. Phys. D* **29**, 1902005 (2020), arXiv:2004.05590 [gr-qc].
- [15] J. Crowder and N. J. Cornish, Beyond LISA: Exploring future gravitational wave missions, *Phys. Rev. D* **72**, 083005 (2005), arXiv:gr-qc/0506015.
- [16] S. Kawamura *et al.*, The Japanese space gravitational wave antenna DECIGO, *Class. Quant. Grav.* **23**, S125 (2006).
- [17] J. D. Romano and N. J. Cornish, Detection methods for stochastic gravitational-wave backgrounds: a unified treatment, *Living Rev. Rel.* **20**, 2 (2017), arXiv:1608.06889 [gr-qc].
- [18] K. Schmitz, New Sensitivity Curves for Gravitational-Wave Signals from Cosmological Phase Transitions, *JHEP* **01**, 097, arXiv:2002.04615 [hep-ph].
- [19] P. Amaro-Seoane, H. Audley, S. Babak, and et al (LISA Team), Laser Interferometer Space Antenna, arXiv e-prints, arXiv:1702.00786 (2017).
- [20] W.-R. Hu and Y.-L. Wu, The Taiji Program in Space for gravitational wave physics and the nature of gravity, *Natl. Sci. Rev.* **4**, 685 (2017).
- [21] J. Luo *et al.* (TianQin Team), TianQin: a space-borne gravitational wave detector, *Class. Quant. Grav.* **33**, 035010 (2016), arXiv:1512.02076 [astro-ph.IM].
- [22] W.-H. Ruan, C. Liu, Z.-K. Guo, Y.-L. Wu, and R.-G. Cai, The LISA-Taiji network, *Nature Astron.* **4**, 108 (2020), arXiv:2002.03603 [gr-qc].
- [23] G. Wang, W.-T. Ni, W.-B. Han, S.-C. Yang, and X.-Y. Zhong, Numerical simulation of sky localization for LISA-TAIJI joint observation, *Phys. Rev. D* **102**, 024089 (2020), arXiv:2002.12628.
- [24] H. Omiya and N. Seto, Searching for anomalous polarization modes of the stochastic gravitational wave background with LISA and Taiji, *Phys. Rev. D* **102**, 084053 (2020), arXiv:2010.00771 [gr-qc].
- [25] N. Seto, Gravitational Wave Background Search by Correlating Multiple Triangular Detectors in the mHz Band, *Phys. Rev. D* **102**, 123547 (2020), arXiv:2010.06877 [gr-qc].
- [26] G. Orlando, M. Pieroni, and A. Ricciardone, Measuring Parity Violation in the Stochastic Gravitational Wave Background with the LISA-Taiji network, (2020), arXiv:2011.07059 [astro-ph.CO].
- [27] R. Wang, W.-H. Ruan, Q. Yang, Z.-K. Guo, R.-G. Cai, and B. Hu, Hubble parameter estimation via dark sirens with the LISA-Taiji network, (2020), arXiv:2010.14732 [astro-ph.CO].
- [28] L.-F. Wang, S.-J. Jin, J.-F. Zhang, and X. Zhang, Forecast for cosmological parameter estimation with gravitational-wave standard sirens from the LISA-Taiji network, (2021), arXiv:2101.11882 [gr-qc].
- [29] G. Wang and W.-B. Han, Observing gravitational wave polarizations with the LISA-TAIJI network, *Phys. Rev. D* **103**, 064021 (2021), arXiv:2101.01991 [gr-qc].
- [30] R. Wang, W.-H. Ruan, Q. Yang, Z.-K. Guo, R.-G. Cai, and B. Hu, Hubble parameter estimation via dark sirens with the LISA-Taiji network, (2020), arXiv:2010.14732 [astro-ph.CO].
- [31] G. Wang and W.-T. Ni, Numerical simulation of time delay interferometry for TAIJI and new LISA, *Res. Astron. Astrophys.* **19**, 058 (2019), arXiv:1707.09127 [astro-ph.IM].
- [32] G. Wang and W.-T. Ni, Time-delay Interferometry for ASTROD-GW, *Chin. Astron. Astrophys.* **36**, 211 (2012), and references therein.
- [33] G. Wang and W.-T. Ni, Numerical simulation of time delay interferometry for NGO/eLISA, *Class. Quant. Grav.* **30**, 065011 (2013), arXiv:1204.2125 [gr-qc].
- [34] G. Wang and W.-T. Ni, Orbit optimization for ASTROD-GW and its time delay interferometry with two arms using CGC ephemeris, *Chin. Phys. B* **22**, 049501 (2013), arXiv:1205.5175 [gr-qc].

- [35] S. V. Dhurandhar, W. T. Ni, and G. Wang, Numerical simulation of time delay interferometry for a LISA-like mission with the simplification of having only one interferometer, *Adv. Space Res.* **51**, 198 (2013), arXiv:1102.4965 [gr-qc].
- [36] G. Wang and W.-T. Ni, Orbit optimization and time delay interferometry for inclined ASTROD-GW formation with half-year precession-period, *Chin. Phys.* **B24**, 059501 (2015), arXiv:1409.4162 [gr-qc].
- [37] G. Wang, W.-T. Ni, and W.-B. Han, Revisiting time delay interferometry for unequal-arm LISA and TAIJI, (2020), arXiv:2008.05812 [gr-qc].
- [38] G. Wang, W.-T. Ni, W.-B. Han, and C.-F. Qiao, Algorithm for TDI numerical simulation and sensitivity investigation, (2020), arXiv:2010.15544 [gr-qc].
- [39] F. B. Estabrook and H. D. Wahlquist, Response of Doppler spacecraft tracking to gravitational radiation., *General Relativity and Gravitation* **6**, 439 (1975).
- [40] H. Wahlquist, The Doppler response to gravitational waves from a binary star source., *General Relativity and Gravitation* **19**, 1101 (1987).
- [41] M. Vallisneri, J. Crowder, and M. Tinto, Sensitivity and parameter-estimation precision for alternate LISA configurations, *Class. Quant. Grav.* **25**, 065005 (2008), arXiv:0710.4369 [gr-qc].
- [42] M. Vallisneri and C. R. Galley, Non-sky-averaged sensitivity curves for space-based gravitational-wave observatories, *Class. Quant. Grav.* **29**, 124015 (2012), arXiv:1201.3684 [gr-qc].
- [43] M. Tinto and M. E. da Silva Alves, LISA Sensitivities to Gravitational Waves from Relativistic Metric Theories of Gravity, *Phys. Rev. D* **82**, 122003 (2010), arXiv:1010.1302 [gr-qc].
- [44] T. A. Prince, M. Tinto, S. L. Larson, and J. W. Armstrong, The LISA optimal sensitivity, *Phys. Rev. D* **66**, 122002 (2002), arXiv:gr-qc/0209039 [gr-qc].
- [45] M. Otto, G. Heinzel, and K. Danzmann, TDI and clock noise removal for the split interferometry configuration of LISA, *Class. Quant. Grav.* **29**, 205003 (2012).
- [46] M. Otto, *Time-Delay Interferometry Simulations for the Laser Interferometer Space Antenna*, Ph.D. thesis, Leibniz U., Hannover (2015).
- [47] M. Tinto and O. Hartwig, Time-Delay Interferometry and Clock-Noise Calibration, *Phys. Rev. D* **98**, 042003 (2018), arXiv:1807.02594 [gr-qc].
- [48] Z. Luo, Z. Guo, G. Jin, Y. Wu, and W. Hu, A brief analysis to Taiji: Science and technology, *Results in Physics* **16**, 102918 (2020).
- [49] C. Cutler and É. E. Flanagan, Gravitational waves from merging compact binaries: How accurately can one extract the binary's parameters from the inspiral waveform?, *Phys. Rev. D* **49**, 2658 (1994), arXiv:gr-qc/9402014 [gr-qc].
- [50] C. Cutler, Angular resolution of the LISA gravitational wave detector, *Phys. Rev.* **D57**, 7089 (1998), arXiv:gr-qc/9703068 [gr-qc].
- [51] M. Vallisneri, Use and abuse of the Fisher information matrix in the assessment of gravitational-wave parameter-estimation prospects, *Phys. Rev.* **D77**, 042001 (2008), arXiv:gr-qc/0703086 [GR-QC].
- [52] K. A. Kuns, H. Yu, Y. Chen, and R. X. Adhikari, Astrophysics and cosmology with a decihertz gravitational-wave detector: TianGO, (2019), arXiv:1908.06004 [gr-qc].
- [53] S. Khan, S. Husa, M. Hannam, F. Ohme, M. Pürrer, X. J. Forteza, and A. Bohé, Frequency-domain gravitational waves from nonprecessing black-hole binaries. II. A phenomenological model for the advanced detector era, *Phys. Rev. D* **93**, 044007 (2016), arXiv:1508.07253 [gr-qc].
- [54] K. Chatziioannou, N. Yunes, and N. Cornish, Model-independent test of general relativity: An extended post-Einsteinian framework with complete polarization content, *Phys. Rev. D* **86**, 022004 (2012), arXiv:1204.2585 [gr-qc].
- [55] K. Chatziioannou, N. Yunes, and N. Cornish, Erratum: Model-independent test of general relativity: An extended post-einsteinian framework with complete polarization content [phys. rev. d 86, 022004 (2012)], *Phys. Rev. D* **95**, 129901 (2017).
- [56] C. M. Will, Bounding the mass of the graviton using gravitational wave observations of inspiralling compact binaries, *Phys. Rev. D* **57**, 2061 (1998), arXiv:gr-qc/9709011.
- [57] C. M. Will and N. Yunes, Testing alternative theories of gravity using LISA, *Class. Quant. Grav.* **21**, 4367 (2004), arXiv:gr-qc/0403100.
- [58] E. Berti, A. Buonanno, and C. M. Will, Testing general relativity and probing the merger history of massive black holes with LISA, *Class. Quant. Grav.* **22**, S943 (2005), arXiv:gr-qc/0504017.
- [59] A. Stavridis and C. M. Will, Bounding the mass of the graviton with gravitational waves: Effect of spin precessions in massive black hole binaries, *Phys. Rev. D* **80**, 044002 (2009), arXiv:0906.3602 [gr-qc].
- [60] K. G. Arun and C. M. Will, Bounding the mass of the graviton with gravitational waves: Effect of higher harmonics in gravitational waveform templates, *Class. Quant. Grav.* **26**, 155002 (2009), arXiv:0904.1190 [gr-qc].
- [61] D. Keppel and P. Ajith, Constraining the mass of the graviton using coalescing black-hole binaries, *Phys. Rev. D* **82**, 122001 (2010), arXiv:1004.0284 [gr-qc].
- [62] K. Yagi and T. Tanaka, Constraining alternative theories of gravity by gravitational waves from precessing eccentric compact binaries with LISA, *Phys. Rev. D* **81**, 064008 (2010), [Erratum: *Phys. Rev. D* **81**, 109902 (2010)], arXiv:0906.4269 [gr-qc].
- [63] N. Cornish, L. Sampson, N. Yunes, and F. Pretorius, Gravitational Wave Tests of General Relativity with the Parameterized Post-Einsteinian Framework, *Phys. Rev. D* **84**, 062003 (2011), arXiv:1105.2088 [gr-qc].
- [64] E. E. Flanagan, The Sensitivity of the laser interferometer gravitational wave observatory (LIGO) to a stochastic background, and its dependence on the detector orientations, *Phys. Rev. D* **48**, 2389 (1993), arXiv:astro-ph/9305029.
- [65] N. Christensen, Measuring the stochastic gravitational radiation background with laser interferometric anten-

- nas, Phys. Rev. D **46**, 5250 (1992).
- [66] J. T. Whelan, W. G. Anderson, M. Casquette, M. C. Diaz, I. S. Heng, M. McHugh, J. D. Romano, J. Torres Charlie W., R. M. Trejo, and A. Vecchio, Progress on stochastic background search codes for LIGO, Class. Quant. Grav. **19**, 1521 (2002), arXiv:gr-qc/0110019.
- [67] M. R. Adams and N. J. Cornish, Discriminating between a Stochastic Gravitational Wave Background and Instrument Noise, Phys. Rev. D **82**, 022002 (2010), arXiv:1002.1291 [gr-qc].
- [68] W.-T. Ni, ASTROD-GW: Overview and Progress, Int. J. Mod. Phys. D **22**, 1341004 (2013), arXiv:1212.2816 [astro-ph.IM].
- [69] J. Baker *et al.*, Space Based Gravitational Wave Astronomy Beyond LISA, (2019), arXiv:1907.11305 [astro-ph.IM].
- [70] A. Sesana *et al.*, Unveiling the Gravitational Universe at μ -Hz Frequencies, (2019), arXiv:1908.11391 [astro-ph.IM].